Two-Step Water Splitting Using Mixed-Metal Ferrites: Thermodynamic Analysis and Characterization of Synthesized Materials

ARTICLE · OCTOBER 2008

CITATIONS
14

READS
44

1 AUTHOR:

Mark D Allendorf
Sandia National Laboratories
213 PUBLICATIONS **8,687** CITATIONS

SEE PROFILE

Article

Two-Step Water Splitting Using Mixed-Metal Ferrites: Thermodynamic Analysis and Characterization of Synthesized Materials

Mark D. AllendorfRichard B. Diver, Nathan P. Siegel, and James E. Miller

Energy Fuels, **2008**, 22 (6), 4115-4124 • Publication Date (Web): 23 October 2008

Two-Step Water Splitting Using Mixed-Metal Ferrites: Thermodynamic Analysis and Characterization of Synthesized Materials

Mark D. Allendorf*

Sandia National Laboratories, Livermore, California 94551-0969

Richard B. Diver, Nathan P. Siegel, and James E. Miller

Sandia National Laboratories, 1515 Eubank, S.E., Albuquerque, New Mexico 87123

Received June 24, 2008. Revised Manuscript Received August 22, 2008

We report a comprehensive thermodynamic analysis of thermal oxidation−reduction cycles for producing hydrogen that use metal ferrites with the spinel structure (MFe_2O_4; M = Fe, Co, Ni, and Zn) as the redox material. Solution phases (both solid and liquid) were included in the calculations as well as the expected line compounds. Omitting solution phases, whose existence is experimentally well-documented, has a very significant impact upon the results of the calculations. Thermodynamic modeling of the three important material-related aspects of the process was performed, including synthesis of the ferrite materials from bulk oxides, thermal reduction at high temperatures, and reoxidation by reaction with steam. An experimental investigation of the $Ni_xFe_{3-x}O_4$ system was performed to provide compositional data for comparison to model predictions. The results indicate that the Fe/Ni ratio, thermal reduction reaction kinetics, and the specifics of the cooling process affect the composition of the synthesized material. In particular, the presence of oxygen in the atmosphere during the cooling period following calcination substantially alters the sample composition. Predicted compositions following thermal reduction indicate that the stabilities are $Fe_3O_4 > CoFe_2O_4 \sim NiFe_2O_4 > ZnFe_2O_4$ and that the zinc-substituted ferrite is less desirable for solar hydrogen generation because of the high vapor pressure of zinc. Finally, modeling of the water oxidation step shows that efficient reoxidation to the original ferrite is thermodynamically feasible in all cases. We conclude that the temperature history and level of background O_2 present will affect both the phase purity of the initially formed material and the stability of the composition over the course of thermal cycling.

Introduction

Thermochemical cycles using metal oxides with the spinel structure (MFe_2O_4; also called ferrites) are a promising method for producing hydrogen using solar energy to drive a two-step water-splitting cycle.[1,2] These cycles consist of a thermal reduction step (TR; reaction 1), in which solar energy is used to reduce the Fe^{III} to the Fe^{II} state with the release of O_2, followed by a water oxidation step (WO; reaction 2), in which the reduced oxide reacts with steam to form hydrogen and regenerate the ferrite.

$$MFe_2O_4 \overset{\Delta}{\leftrightarrow} MO + 2FeO + 0.5O_2 \quad (1)$$

$$MO + 2FeO + H_2O \leftrightarrow MFe_2O_4 + H_2 \quad (2)$$

These equations represent only the redox reactions involving line (i.e., stoichiometric) compounds. In fact, solid solutions of various metal oxides are also formed in reaction 1. In the simplest case, M = Fe and the redox system comprises the reduction of iron ferrite (magnetite) to ferric oxide (wustite). Hydrogen production using Fe_3O_4, originally proposed by Nakamura,[3] is not practical, because the temperatures required to drive the TR step (2100 K) result in sintering of the material or formation of a liquid phase, leading to the loss of oxide by vaporization and irreversibility. Also, high temperature TR can lead to significant thermal losses and reduce the overall efficiency of the solar reactor. Supporting Fe_3O_4 on yttria-stabilized zirconia reduces this problem.[4] Alternative redox systems, in which M is either a transition metal or an alkaline earth metal, have been proposed to decrease the temperature required for reduction. These mixed-metal ferrites, including the systems with M = Mn,[5] Co,[6] Ni,[7,8] and Zn,[9,10] are now receiving considerable attention. These chemistries have been recently reviewed.[11]

* To whom correspondence should be addressed. Telephone: (925) 294-2895. Fax: (925) 294-3282. E-mail: mdallen@sandia.gov.

(1) Steinfeld, A. *Sol. Energy* **2005**, *78*, 603–615.
(2) Kodama, T. *Prog. Energy Combust. Sci.* **2003**, *29*, 567–597.
(3) Nakamura, T. *Sol. Energy* **1977**, *19*, 467.
(4) Kodama, T.; Nakamuro, Y.; Mizuno, T. *J. Sol. Energy Eng.* **2006**, *128*, 3.
(5) Ehrensberger, K.; Frei, A.; Kuhn, P.; Oswald, H. R.; Hug, P. *Solid State Ionics* **1995**, *78*, 151–160.
(6) Kodama, T.; Kondoh, Y.; Yamamoto, R.; Andou, H.; Satou, N. *Sol. Energy* **2005**, *78*, 623–631.
(7) Ishihara, H.; Kaneko, H.; Yokoyama, T.; Fuse, A.; Hasegawa, N.; Tamaura, Y. *Solar Eng.* **2005**, 687.
(8) Aoki, H.; Kaneko, H.; Hasegawa, N.; Ishihara, H.; Takahashi, Y.; Suzuki, A.; Tamaura, Y. International Solar Energy Conference (ISEC), Portland, OR, 2004; paper ISEC2004-65068.
(9) Tamaura, Y.; Kojima, N.; Hasegawa, N.; Inoue, M.; Uehara, R.; Gokon, N.; Kaneko, H. *Int. J. Hydrogen Energy* **2001**, *26*, 917–922.
(10) Tamaura, Y.; Kaneko, H. *Sol. Energy* **2005**, *78*, 616–622.
(11) Kodama, T.; Gokon, N. *Chem. Rev.* **2007**, *107*, 4048.

10.1021/ef8005004 CCC: $40.75
Published on Web 10/23/2008

A number of reactor concepts using solar-driven redox of metal-oxide systems to generate hydrogen are currently under consideration.[11] These include rotary-type reactors,[12] fluidized beds,[13] and reactors incorporating multichannel honeycomb structures[14] and ceramic foams coated with ferrite.[15] Recently, we described a novel solar-driven heat engine that uses heat recovery to achieve acceptable thermal efficiencies.[16−18] The counter-rotating-ring receiver/reactor/recuperator or CR5 consists of a stack of counter-rotating rings to which are attached fins fabricated from an active metal-oxide ceramic. As these rings rotate, metal-oxide material passes alternately through a high-temperature TR zone and a lower temperature WO zone. Because the fins counter-rotate, hot surfaces from the TR zone radiate to cooler fins passing from the WO zone; thus, sensible heat is recovered internally, reducing the overall energy input requirements. In each of these concepts, the selected thermal redox material and the choice of operating temperatures play a critical role in the efficiency and durability of the technology. Modeling using thermodynamic equilibrium codes can provide key insights into these process aspects and guide both design and material selection. To date, however, thermodynamic analysis of these systems has been limited in scope.[9,19,20]

In this paper, we report a thermodynamic analysis of the ferrite systems, in which M = Fe, Co, Ni, and Zn; limited results for M = Mg are also included. Equilibrium calculations based on minimization of the Gibbs free energy were performed and include thermodynamic data for non-ideal solid- and liquid-phase solutions that can form. The results indicate that, in contrast to the relatively simple picture of line compounds suggested by reactions 1 and 2, liquid and solid solution phases are the major products of reaction 1. The formation of liquid-phase products is predicted to occur at much lower temperatures than if solution phases are not included in the calculation. Thus, inclusion of solution phases in the thermodynamic model is essential to accurately simulate this high-temperature chemistry. Using this comprehensive thermodynamic approach, we modeled the synthesis of mixed-metal ferrites and show that the phase composition of calcined samples is a strong function of both the initial Fe/M mole ratio, the gas-phase composition, and the calcination temperature. These results are compared to measured compositions for a set of representative NiO/FeO mixtures, confirming the equilibrium model predictions but also showing that the final product phases depend upon whether the gas present during cool down contains oxygen. In addition, we modeled the TR step to compare the relative merits of the four transition-metal ferrites. Finally, predicted equilibrium compositions for the WO step indicate, as expected, that the reduction of all four ferrites is reversible across a broad temperature range, enabling efficient production of hydrogen from steam.

Table 1. Species Included in Thermodynamic Calculations

gases			pure liquids	pure solids
Ar	N_2	Fe	Fe	Fe
H_2	NO	Co	Mg	Mg
O_2	NO_2	Ni	Co	Co
O	Mg	Zn	Ni	Ni
H_2O	Mg_2	FeO	Zn	Zn
CO		NiO	(FeO)[a]	
CO_2		ZnO		Fe_2O_3 (hematite)
solution phases				MgO
spinel	zincite			FeO (wustite)[b]
metal oxides (MeO)				
slag				

[a] Only included when the slag phase was not included. [b] Included only if the MeO solution phase was not included.

Computational Methods

Thermodynamic calculations were performed using the FactSage program,[21] version 5.4.1 or higher. Thermodynamic data for solution phases were obtained from version 5.3 of the FactSage oxide solution database,[21] which were assessed over a range of conditions that encompass the systems of interest here.[21−25] Species and solutions included in the calculations are listed in Table 1. The following solutions were included in the calculations: (1) Spinel (Fe_3O_4 and $M_xFe_{3-x}O_4$, M = Co, $x = 0-3$; Ni, $x = 0-1$; or Zn, $x = 0-1$; designated "spinel"). The model used to describe this phase is the compound energy formalism of Hillert et al., in which Fe^{II} and Fe^{III} cations are distributed over tetrahedral and octahedral sites, as well as vacancies on the octahedral sites to permit oxygen nonstoichiometry.[26,27] (2) Metal-oxide solid solution phase, designated "MeO". This solution was modeled by Pelton and co-workers as a simple random mixture of M^{II} (M = Mg, Co, Ni, and Zn), Fe^{II}, and Fe^{III} on cation sites with polynomial excess Gibbs energy terms.[24,25,28] The Fe^{III} on cation sites allows for a representation of the hyperstoichiometry (i.e., O/Fe ratios > 1.0) in the wustite and metal-substituted wustite regions of the phase diagram. For the modeling of zinc-containing systems, the MeO phase was used for conditions that are dilute in Zn. In all other cases, the "zincite" solution, which models zincite solid solutions containing dilute Fe^{II} up to and including pure ZnO, was used. The zincite model is similar that used for the MeO solution. (3) Slag, a molten oxide phase. This phase was modeled using the modified quasichemical model,[29] which accounts for short-range ordering and interactions of second nearest neighbor cations in an ionic melt. Further details

(12) Kaneko, H.; Miura, T.; Fuse, A.; Ishihara, H.; Taku, S.; Fukuzumi, H.; Naganuma, Y.; Tamaura, Y. *Energy Fuels* **2007**, *21*, 2287.
(13) Gokon, N.; Mizuno, T.; Takahashi, S.; Kodama, T. International Solar Energy Conference (ISEC), Denver, CO, 2006.
(14) Roeb, M.; Sattler, C.; Kluser, R.; Monnerie, N.; de Oliveira, L.; Konstandopoulos, A. G.; Agrafiotis, C.; Zaspalis, V. T.; Nalbandian, L.; Steele, A.; Stobbe, P. *J. Solar Energy Eng.* **2006**, *128*, 125.
(15) Kodama, T.; Hasegawa, T.; Nagasaki, A.; Gokon, N. American Society of Mechanical Engineers (ASME) Energy Sustainability Conference, Long Beach, CA, 2007.
(16) Diver, R. B., Jr.; Miller, J. A.; Allendorf, M. D.; Siegel, N. P.; Hogan, R. E. *Proc. ASME Int. Solar Eng. Conf.* **2007**, 301.
(17) Miller, J. E.; Allendorf, M. D.; Diver, R. B.; Evans, L. R.; Siegel, N. P.; Stuecker, J. N. *J. Mater. Sci.* **2008**, *43*, 4714–4728.
(18) Miller, J. E.; Evans, L. R.; Stuecker, J. N.; Allendorf, M. D.; Siegel, N. P.; Diver, R. B. *Proc. ASME Int. Solar Eng. Conf.* **2007**, 311.
(19) Charvin, P.; Abanades, S.; Flamant, G.; Lemort, F. *Energy* **2007**, *32*, 1124.
(20) Lundberg, M. *Int. J. Hydrogen Energy* **1993**, *18*, 369.
(21) Bale, C. W.; Chartrand, P.; Degterov, S. A.; Eriksson, G.; Hack, K.; Mahfoud, R. B.; Melançon, J.; Pelton, A. D.; Petersen, S. *Calphad* **2002**, *26*, 189–228.
(22) Decterov, S. A.; Jung, I.-H.; Jak, E.; Kang, Y.-B.; Hayes, P.; Pelton, A. D., VII International Conference on Molten Slags and Salts, The South African Institute of Mining and Metallurgy, Marshalltown, South Africa, 2004.
(23) Decterov, S. A.; Jung, I.-H.; Pelton, A. D. *J. Am. Ceram. Soc.* **2002**, *85*, 2903.
(24) Decterov, S. A.; Jak, E.; Hayes, P. C.; Pelton, A. D. *Metall. Mater. Trans. B* **2001**, *32*, 643–657.
(25) Jung, I.-H.; Decterov, S. A.; Pelton, A. D.; Kim, H.-M.; Kang, Y.-B. *Acta Mater.* **2004**, *52*, 507–519.
(26) Frisk, K.; Selleby, M. *J. Alloys Compd.* **2001**, *320*, 177.
(27) Hillert, M. *J. Alloys Compd.* **2001**, *320*, 161.
(28) Jung, I.-H.; Decterov, S. A.; Pelton, A. D. *J. Phys. Chem. Solids* **2004**, *65*, 1683.
(29) Pelton, A. D. *Metall. Mater. Trans. A* **2001**, *32*, 1355.

of the models used to generate these data can be found elsewhere for the Fe−Co−O,[25] Fe−Ni−O,[21] and Fe−Zn−O[24] systems and for the oxide solid solution[22,23] and slag[22] phases. Hematite (Fe_2O_3) was included as a pure solid, and its data were obtained from the Fact 5.3 database. Using these data and the FactSage program, we can reproduce published phase diagrams for the systems of interest. All computations were performed for the condition of 1.0 atm total pressure.

Experimental Methods

Nickel-substituted ferrites were synthesized by co-precipitating the metals from nitrate solutions with reagent-grade ammonium hydroxide and calcining the washed precipitate. An aqueous solution of the nitrate salts was slowly added to an approximately equal volume of an ammonium hydroxide solution with a hydroxide ion content that was 1.5 times the nitrate ion content to be added. The resulting precipitate was filtered and washed with water until the pH of the filtrate was measured to be 7 or less. In this procedure, a small amount of the nickel is lost to the solution; a slight blue tint is typically evident in the filtrate, particularly for the higher nickel concentrations ($x = 0.95$ and 1.4). The recovered filter cake was dried at 80 °C for at least 12 h, divided, and calcined. Three different ferrite stoichiometries were prepared: $Ni_xFe_{(3-x)}O_4$ with $x = 0.5$, 0.95, and 1.4. After the initial preparation steps, samples were divided and subjected to different calcination conditions. Two different calcination procedures were employed. In the first case, the samples were calcined for 2 h at 900, 1100, 1250, or 1400 °C and cooled to ambient, both in air. In the second case, the samples were heated and calcined for 2 h in air. Prior to cooling, however, the air flow was replaced with an inert argon purge to ensure that any reduced metals were not reoxidized during the cool-down phase of the furnace temperature ramp. A total of 24 samples resulted from this procedure. We find experimentally that TR and WO occur on this time scale at temperatures of 1100−1500 °C.[17]

X-ray diffraction analysis of the ferrites was performed on a Siemens D500 diffractometer with a graphite-diffracted beam monochromator using Cu Kα radiation operated at 40 kV and 30 mA. Scans were typically from 15−65° 2θ at 0.02° step width for 3 s/step. Prior to analysis, the particulate metal oxide solids were ground to a fine powder by mortar and pestle. Rietveld quantitation was performed using Topas3 software from Bruker AXS, Inc.

Results and Discussion

Importance of Solution Phases. Reactions 1 and 2 above are expressions that do not explicitly account for the formation of either solid- or liquid-phase solutions. In actuality, multiple phases can form that have a major effect on the behavior of the system. Previously published thermodynamic analyses did not include solution phases.[9,19,20] Our calculations demonstrate that neglecting these phases results in thermodynamic predictions for ferrite systems (particularly melting points and H_2 yields) that are considerably different from the results obtained when they are included. Because the formation of solution phases is experimentally observed and indicated on phase diagrams for these systems,[30] we conclude that equilibrium predictions that do not account for both solid- and liquid-phase solutions are incorrect.

To illustrate the effect of including solution phases, we now describe calculations for the case of thermal reduction in the relatively simple iron spinel system (Fe_3O_4), but similar conclusions can be reached for any of the ferrite systems considered later in this paper. We consider three cases: case 1, all available solution phases included (spinel, MeO, and slag); case 2, slag phase in case 1 replaced by liquid FeO; and case 3, no metal oxide solution phases other than the spinel phase.

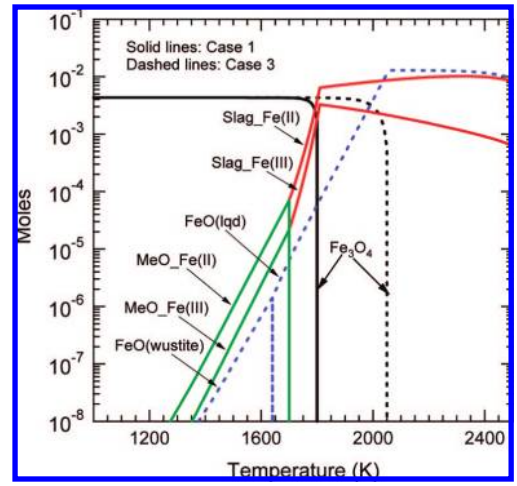

Figure 1. Effect of including solution phases: comparison of cases 1 and 3 (see the text). Vertical lines indicate solid−liquid phase transitions [e.g., between FeO(wustite) and FeO(lqd)]. Black, spinel phase; blue, FeO (solid- or liquid-phase wustite); green, components of the MeO metal-oxide solid solution; red, components of the slag phase. Solid lines, case 1; dashed lines, case 3. The vertical axis plots the moles of each phase (or component of a phase) formed at equilibrium. The input conditions for each calculation were 1.0 g (4.32×10^{-3} mol) of Fe_3O_4 in an atmosphere of 1.0 mol of Ar at 1 atm.

We computed the combined condensed- and gas-phase equilibrium for each of these cases, using the input conditions 1.0 g (4.32×10^{-3} mol) of Fe_3O_4 in an atmosphere of 1.0 mol of N_2 at 1 atm, which are similar to small-scale experiments reported in the literature. The activity of gas-phase O_2 was allowed to vary, as it would under TR conditions.

The calculations predict two important consequences of including solution phases in the calculations. First, the temperature at which the ferrite decomposes is substantially reduced when solution phases (MeO and slag) are included. Under TR conditions, the oxygen activity is not fixed (i.e., the partial pressure of oxygen can vary), causing ferrite compounds to lose oxygen rather than melting congruently and leading to solutions of overall composition MFe_2O_{4-x}. A solid solution of oxides (described here by the MeO phase) forms at low temperatures, followed at higher temperatures by the formation of the liquid slag phase. The results in Figure 1 show that the decomposition temperature of Fe_3O_4 is much higher in the absence of the MeO and slag phases. In the absence of these phases (case 3), the only liquid that can form is FeO, which melts at 1643 K. Our thermodynamic model predicts that the Fe_3O_4 decomposition temperature T_d (the temperature in which no Fe_3O_4 remains) is 2040 K. Allowing Fe_3O_4 to decompose to the MeO phase in the calculation decreases T_d to 1900 K (case 2; not shown). Including both the slag and MeO phases (case 1) decreases T_d further to 1800 K, with the solid solution MeO forming at $T <$ 1700 K. The molten slag phase forms at $T \geq 1700$ K, above the melting point of pure FeO. In general, we find that including solution phases decreases the ferrite decomposition temperature, while also shifting to higher temperatures the point at which a molten phase forms.

The second consequence is that, under TR conditions, the inclusion of solution phases allows for hyperstoichiometry; therefore, Fe^{III} forms in the MeO and slag phases, which is not possible in case 3 when only stoichiometric FeO is included in the calculation. At 1800 K (T_d in case 1), the mole fraction of Fe^{III} in the slag phase is ~0.49 (note that in Figure 1 the vertical axis units are moles; we compute the mole fraction from the

(30) The American Ceramic Society. *Phase Diagrams for Ceramists*; The American Ceramic Society: Westerville, OH, 1964−1996; Vol. 1−12.

FactSage results). This value decreases with increasing temperature but is still 0.13 at 2500 K. Because Fe^{III} does not react with H_2O to yield H_2, the net effect is to reduce the predicted overall efficiency of the process. Thus, the neglect of solution phases in case 3 leads to predicted H_2 production efficiencies that are too high.

One factor that was not considered in this modeling is the influence of ceramic supports, such as zirconia. It is well-known that doping with iron can stabilize zirconia.[31−33] The solubility limit of Fe_2O_3 in cubic ZrO_2 is reported to be 25%.[32] In addition, there is evidence that ZrO_2 is not a chemically passive material in the presence of iron and that iron cations can diffuse into this lattice and undergo redox reactions. Unfortunately, the thermodynamic data are insufficient. The FactSage database includes data for a solid solution containing dilute Fe^{II} in ZrO_2 but not Fe^{III}; therefore, we were unable to model redox reactions involving these cations. Thermodynamic data in the literature are also sparse, although phase diagrams indicating the solution-phase domains have been published.[30] The intriguing evidence of Kodama et al. for a highly reactive Fe-doped form of cubic zirconia that could be used for a two-step water-splitting cycle provides motivation for further investigations.[4]

As a result of these observations, we employ the full set of applicable solution models (case 1, with the addition of the zincite solution for situations involving zinc) in all further calculations described below.

Synthesis of Ferrites. Mixed-metal ferrites can be synthesized by several methods, including precipitation from solutions containing metal salts followed by calcination under a reducing atmosphere,[34] the "aerial oxidation" method of Kodama et al.,[6,35] and physical mixing of oxide powders. In all cases, the resulting materials, either powders, gels, or precipitates, must first be heated (often in an inert atmosphere) to remove volatile compounds and then calcined at high temperature in air to drive the solid-state reactions toward completion. Equilibrium modeling indicates that heating mixtures of metal oxides in air yields compositions that vary as a function of the temperature and input oxide composition. To illustrate this, we assume that all synthetic methods yield a mixture of the metal oxides nMO + (1 − n)FeO after an initial heating step to drive off solvents or other volatile components. Phase equilibria were then computed for the example [nCoO + (3 − n)FeO] ($0.0 < n < 1.5$), with O_2 activity fixed at 0.21 atm (air).

Our modeling indicates that the cobalt−ferrite system is representative of the equilibrium behavior of the other metal ferrite systems examined in this study (M = Mg, Ni, and Zn), in that analogous phases form and the trends with calcination temperature and composition are similar. As seen in Figure 2, there are three dominant phases: Fe_2O_3 (hematite), the spinel phase, and the MeO solid solution. No liquid phases form at any of the temperatures considered (up to 1673 K). The system behavior can be divided into two basic composition regions: the low cobalt region [n(CoO) ≤ 1.00, where n(CoO) is the number of moles of CoO input to the calculation] and the high cobalt region [n(CoO) > 1.00].

In the low-cobalt region, hematite and spinel are the only phases present. As n(CoO) approaches 1.00, the amount of spinel formed increases, while the amount of Fe_2O_3 decreases until, at n(CoO) = 1.00, only stoichiometric spinel ($CoFe_2O_4$) is present. In the high-cobalt region (n(CoO) > 1.00), the spinel phase is gradually replaced by the MeO solid-solution phase. These trends are affected by the temperature. At the highest temperature (1673 K), only the spinel phase forms at n(CoO) ≤ 1.00. At temperatures below 1673 K, however, substantial amounts of Fe_2O_3 are predicted to form. In fact, at 1173 K, Fe_2O_3 is the dominant oxide on a molar basis for n(CoO) ≤ 0.6. Very similar trends are predicted for the other substituted ferrites, as illustrated in Figure 3 for M = Mg, Co, Ni, and Zn at 1673 K. In contrast, when n(CoO) ≥ 1.00, lower temperatures favor the spinel phase. For example, at 1173 K, only spinel is present up to n(CoO) = 1.50. As temperature increases, the MeO phase grows in but does not become dominant until n(CoO) > 1.4 and the temperature reaches 1673 K.

The composition of the solid-solution phases varies as a function of the input MO concentration and depends upon both temperature and the identity of M. The elemental composition of the spinel phase is essentially constant at 1173 K, when M = Ni, while at 1673 K, the fraction of Ni atoms X(Ni) increases linearly with increasing n(NiO) up to 1.0 and then becomes

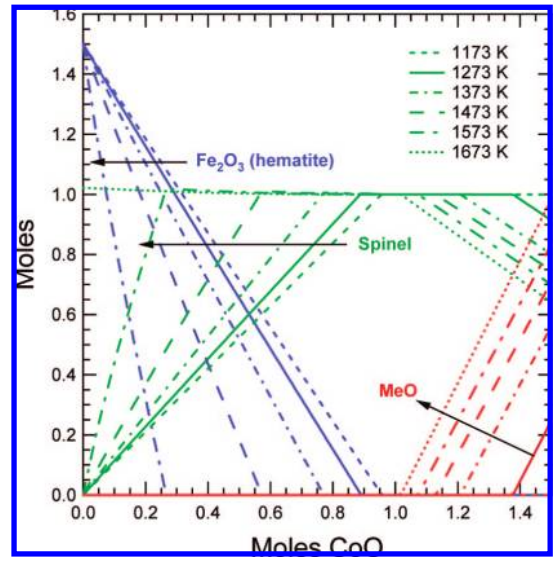

Figure 2. Predicted composition of calcined samples resulting from the mixtures [nCoO + (3 − n)FeO], $n = 0-1.5$ in air, as a function of the temperature. Arrows point in the direction of increasing temperature. Blue, Fe_2O_3; green, spinel; red, MeO phase.

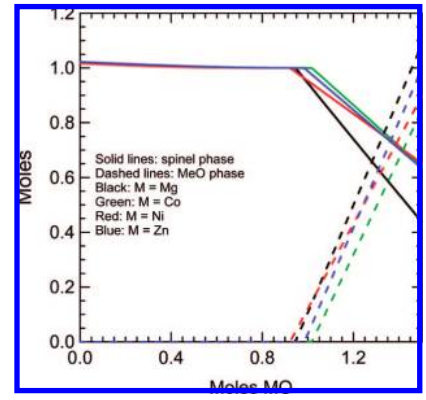

Figure 3. Comparison of the composition of oxide mixtures [nMO + (3 − n)FeO + excess oxygen; M = Mg, Co, Ni, and Zn] calcined at 1673 K as a function of input moles of MO (n).

(31) Berry, F. J.; Loretto, M. H.; Smith, M. R. *J. Solid State Chem.* **1989**, *83*, 91.
(32) Davison, S.; Kershaw, R.; Dwight, K.; Wold, A. *J. Solid State Chem.* **1988**, *73*, 47.
(33) Li, P.; Chen, I. W.; Pennerhahn, J. E. *J. Am. Ceram. Soc.* **1994**, *77*, 118.
(34) Erickson, D. S.; Mason, T. O. *J. Solid State Chem.* **1985**, *59*, 42.
(35) Kodama, T.; Gokon, N.; Yamamoto, R. *Sol. Energy* **2008**, *82*, 73–79.

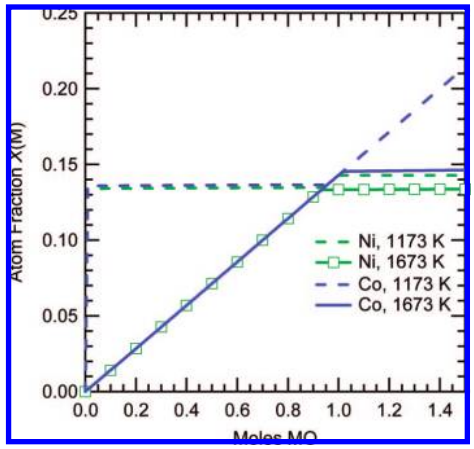

Figure 4. Fraction of Ni or Co atoms in the spinel phase resulting from reacting mixtures nMO + (3 − n)FeO in excess oxygen.

constant (Figure 4).[36] Cobalt appears to be an exception to this. Its behavior at 1673 K is similar to the others. However, for n(CoO) > 1.0 at 1173 K, the spinel composition increases linearly, becoming richer in Co with increasing n(CoO) until the stoichiometry reaches Co_3O_4. This does not occur when M = Mg, Ni, and Zn, because the M_3O_4 stoichiometry does not exist for these metals. The composition of the MeO phase, which only forms in significant amounts when n(MO) > 1.0 (see for example Figure 2), also varies as a function of M (note that, in the case of M = Zn, the zincite phase forms instead of the MeO phase but the behavior is qualitatively similar). For example, when M = Co, the mole fraction of Fe^{III} reaches a maximum of 0.18 at 1673 K. Somewhat lower amounts [$X(Fe^{III}) = 0.10$] are formed at 1673 K for M = Ni. Fe^{III} does not react to produce H_2, as discussed above; therefore, the combination of high calcination temperatures and MO > 1.0 in the reactant mixture should be avoided.

These results suggest two guidelines for synthesis of substituted ferrites. First, high calcination temperatures (1673 K) are required to obtain only the spinel phase at input metal ratios (M/Fe) less than 0.5 [e.g., n(CoO) < 1.0 in Figure 2]. To use lower calcination temperatures, reactant oxide mixtures with M/Fe = 0.45−0.50 (n = 0.95−1.0) should be used. We note that this conclusion agrees with the observations of Han et al., who find that $NiFe_2O_4$ was the best material for a hydrogen thermochemical cycle of those they examined and that calcination at 1373 K in air of a sample with M/Fe = 0.50 produced a $NiFe_2O_4$ sample free of Fe_2O_3 (within the detection limits of XRD).[37] Second, reactant mixtures containing M/Fe > 0.50 [n(MO) > 1.0] have no advantage, because no additional spinel forms beyond the amount required to form stoichiometric MFe_2O_4 and the excess MO cannot be further reduced during the TR step.

Comparison with Experiments. Although the thermodynamic data in the FactSage database[21] used here were obtained by modeling experimental data,[22−25,38] it is not known how closely the methods used to synthesize ferrites for solar hydrogen production approach thermodynamic equilibrium. Consequently, we conducted an experimental investigation to provide data for comparison to the predictions of our thermodynamic model. The nickel ferrite system was chosen for these experiments because our previous thermodynamic analysis[36] as well as experimental

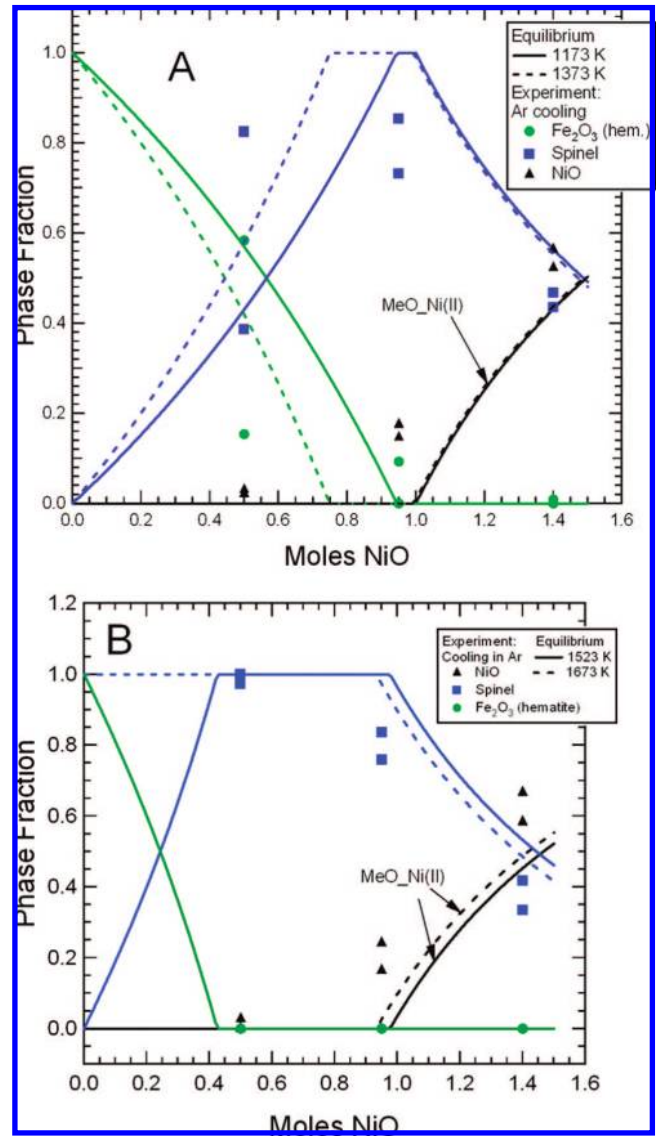

Figure 5. Comparison of equilibrium predictions with measured compositions for samples calcined at various temperatures (A, 1173 and 1373 K; B, 1523 and 1673 K) and then cooled in argon. Symbols indicate composition as measured by XRD, and continuous lines represent equilibrium predictions. The vertical axis indicates the fraction of total sample (molar basis) corresponding to each phase.

investigations[7,8,35,37] suggest that this ferrite may have the best combination of properties for solar hydrogen generation of the metal-substituted ferrites examined thus far.

Two sets of experiments were performed, using precipitates formed from three solutions of iron and nickel nitrates, in which the metal-ion concentrations were adjusted to yield nominal spinel compositions of $Ni_{0.5}Fe_{2.5}O_4$, $Ni_{0.95}Fe_{2.05}O_4$, and $Ni_{1.4}Fe_{1.6}O_4$. In the first set of experiments, the precipitates were calcined in air over a range of temperatures that bracket those typically used for ferrite synthesis (1173, 1373, 1523, and 1673 K) and then cooled to room temperature in dry Ar (Figure 5). The second set of experiments was identical to the first, except that the samples were cooled in air (Figure 6). The corresponding equilibrium predictions are also shown in the figures (for clarity, only the 1173 and 1673 K air-cooled results are displayed).

Two separate calculations were required to simulate the experiments. First, we computed the equilibrium composition at the calcination temperature, using an input composition of x mol of MO, (3 − x) mol of FeO, and a gas phase

(36) Allendorf, M. D., Jr.; Miller, J. E.; Siegel, N. P. *Proc. ASME Int. Solar Eng. Conf.* **2007**, 285.
(37) Han, S. B.; Kang, T. B.; Joo, O. S.; Jung, K. D. *Sol. Energy* **2008**, *81*, 623–628.
(38) Decterov, S.; Pelton, A. D. *J. Phase Equilib.* **2004**, *17*, 476.

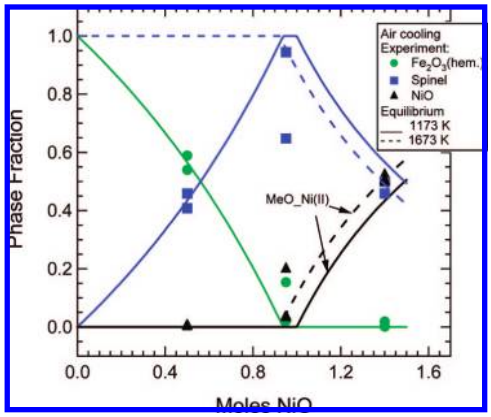

Figure 6. Comparison of equilibrium predictions with the experiment for samples cooled in air (O_2 activity fixed at 0.21 atm). Symbols indicate composition as measured by XRD, and continuous lines represent equilibrium predictions. The vertical axis indicates the fraction of total sample (molar basis) corresponding to each phase.

composed of 3.95 mol of Ar and 1.05 mol of O_2 (approximately equivalent to air). The pressure was held fixed at 1 atm with a fixed O_2 activity of 0.21 atm. The resulting solid-state composition, which in some cases consists of a mixture of two phases, was then saved and used as the input composition for a second equilibrium calculation to simulate the cool-down phase. In this calculation, the equilibrium composition was computed as a function of the temperature using a gas phase at 1 atm and composed of either Ar or air (50 mol). As in the first calculation, the activity of O_2 was fixed at 0.21 atm. In both calculations, all solution phases were included, as in case 1 described above.

The observed compositional trends for argon-cooled samples are in good agreement with the predicted equilibrium composition with respect to the spinel phase and Fe_2O_3. The equilibrium modeling predicts that a nickel-rich (87 mol % of the metal ions) MeO solid solution phase also forms, which we correlate with the observation of NiO by XRD. At the two lower temperatures (Figure 5A), mixtures of Fe_2O_3 and iron−nickel spinel (the exact elemental composition of the spinel phase cannot be determined by XRD) are formed at the composition $x = 0.5$ in $Ni_xFe_{3-x}O_4$. At the near-stoichiometric composition ($x = 0.95$), the samples consist primarily of spinel but with some NiO also present (indicated as MeO_Ni^{II} in Figures 5 and 6). At $x = 1.4$, Fe_2O_3 is absent entirely and the sample is a nearly equimolar mixture of ferrite and NiO (again represented by MeO_Ni^{II} in the model), as predicted by equilibrium. The higher temperature samples (Figure 5B) are entirely free of Fe_2O_3 at all three compositions, also in agreement with equilibrium, and the $x = 0.95$ and 1.40 samples consist of a mixture of spinel and NiO.

When the samples are cooled in air, a different behavior is observed, as seen in Figure 6. In this case, the $x = 0.5$ samples contain Fe_2O_3, regardless of the calcination temperature, and the measured composition is essentially the same at all four temperatures. The $x = 0.95$ samples, on the other hand, contain much less spinel and more NiO and Fe_2O_3 than predicted by equilibrium, but the composition approaches equilibrium as the temperature increases. Finally, the composition of the $x = 1.4$ samples generally agrees with the equilibrium predictions at all temperatures, as is the case for the nitrogen-cooled samples.

These results indicate that the Fe/Ni ratio, reaction kinetics, and the specifics of the cooling process, i.e., the possibility of reoxidation during cooling, all play a role in determining the final composition. In particular, the comparisons between theory and experiment described above suggest that the reaction kinetics depend upon the Fe/Ni ratio and are slower near the ratio of Fe/Ni = 2 ($x = 1.0$) than at values either above or below this. Although not well-documented in the literature, composition-dependent kinetics in the Fe−Ni−O system have been reported[39] and our modeling of TR (discussed below) indicates that metal substitution in Fe_3O_4 makes TR easier by stabilizing the reduction product in solid solution or slag phases.

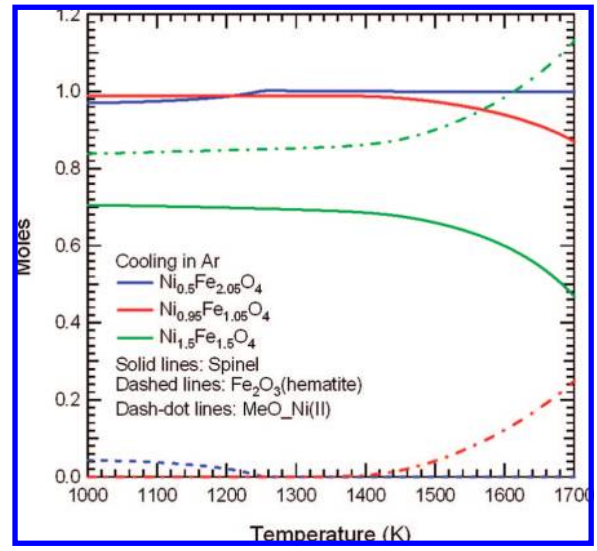

Figure 7. Equilibrium composition for samples calcined at 1673 K and cooled in Ar from oxide mixtures that would yield the nominal stoichiometries shown in the legend. Assuming fast reaction kinetics, the composition of the mixture as the sample is cooled is given by the plot.

These observations can be rationalized by accounting for the temperature-dependent equilibrium composition and making some assumptions concerning the kinetics of the oxidation reactions. To do this, we computed cooling curves that model the evolution of samples following completion of the calcination step. This was performed by (1) computing the phase equilibrium at a fixed calcination temperature for input FeO/NiO mixtures corresponding to the experiments (e.g., 0.95 mol of NiO plus 2.05 mol of FeO in 5.0 mol of air) to simulate calcination and then (2) using the resulting mixture of phases as the input to a second calculation of the equilibrium as a function of the temperature in 50 mol of Ar or air (O_2 activity fixed at 0.21 atm) to simulate cooling. The computed equilibrium cooling curves are shown in Figures 7 and 8 for a sample calcined at 1673 K.

When cooled in an Ar atmosphere (Figure 7), the $x = 0.5$ equilibrium composition of the calcined sample at 1673 K is essentially constant as the temperature decreases to 1000 K; thus, the composition measured for the cooled sample is the same as the 1673 K equilibrium composition. On the other hand, the $x = 1.5$ equilibrium composition changes as the temperature decreases. As a result, the measured compositions of $x = 1.5$ samples are similar regardless of the calcination temperature used (Figure 5). When samples are cooled in air (Figure 8), the $x = 0.5$ equilibrium composition is also temperature-sensitive; therefore, the composition initially formed at the calcination temperature shifts to a lower temperature equilibrium composition until the kinetics are too slow and the composition freezes. Thus, the measured compositions of the $x = 0.5$ samples cooled in air all have roughly the same composition, as do the $x = 1.4$

(39) Paladino, A. E., Jr. *J. Am. Ceram. Soc.* **1959**, *42*, 168.

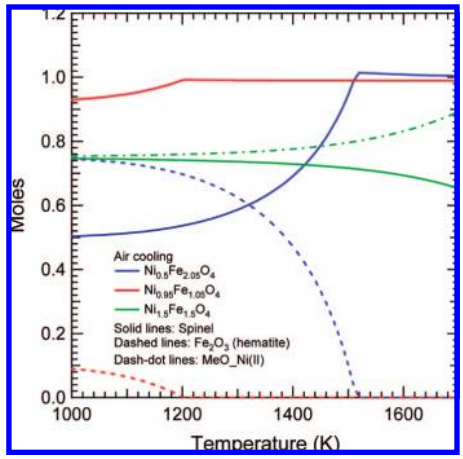

Figure 8. Equilibrium composition predicted for samples calcined at 1673 K and cooled in air from oxide mixtures that would yield the nominal stoichiometries shown in the legend (see the text for details). Assuming fast reaction kinetics, the composition of the mixture as the sample is cooled is given by the plot.

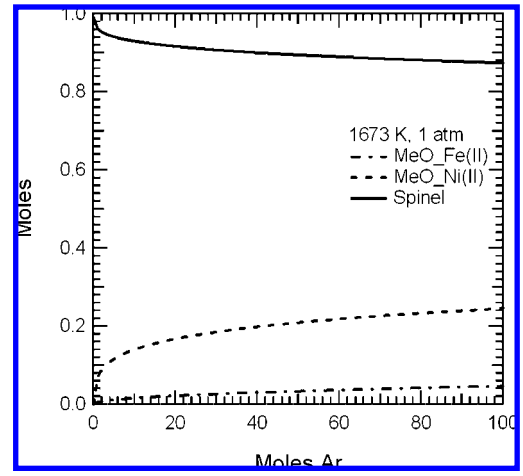

Figure 9. Variation in the composition of a 1 mol sample with nominal composition $Ni_{0.95}Fe_{2.05}O_4$ as a function of the moles of Ar included in the calculation (1673 K).

samples (Figure 6). In summary, off-stoichiometric compositions can be predicted by equilibrium because the chemical reactions occurring during calcination and cooling are fast (on the scale of these experiments). However, in the calculations, one must be careful to account for the presence or absence of oxygen during cool down.

In contrast, for reasons that are not clear, the kinetics of spinel formation during calcination in air appear to be slow when $x = 0.95$. Equilibrium predicts that samples initially formed by calcination in air at any temperature in the range of 1173−1673 K will consist only of the spinel phase (see Figure 2 for the cobalt case; the situation is analogous for nickel). Cooling in air does not alter this (Figure 8) and has only a modest effect on the spinel composition, varying from $NiFe_2O_4$ at 1000 K to $Ni_{0.93}Fe_{2.07}O_4$ at 1700 K. Thus, the presence of NiO and Fe_2O_3 in the air-cooled samples (Figure 6) appears to be due to slow reaction kinetics, i.e., incomplete conversion to the spinel during calcination. Evidently, the oxidation of reactant FeO to Fe_2O_3 is fast relative to the formation of $NiFe_2O_4$ under these conditions.

The situation is different with inert-gas cooling. In this case, equilibrium predicts that inert-gas dilution destabilizes the spinel formed during calcination, leading to a mixture of spinel and an MeO phase that is nickel-rich (Figure 5). In a flowing system, such as the one used here, the continuous stream of inert gas is equivalent to a large dilution of the gas phase, leading to very low oxygen partial pressures and causing nickel oxide to precipitate from the spinel and form (presumably) a higher iron spinel phase (Figure 9).

These results, while limited, demonstrate that phase transformations in ferrite systems are much more complex than are typically appreciated or taken into account. Prior to this work, the operative understanding of chemical reaction and equilibrium in these systems has been considerably oversimplified. It is clear that care must be taken during sample preparation, with regard to both the temperature history and the composition of the atmosphere. This conclusion is consistent with recent experimental observations reported by Charvin et al., who showed that an inert atmosphere is required to prevent reoxidation of Fe^{II} oxide during quenching, following TR of Fe_3O_4 to FeO.[19]

An additional conclusion resulting from this analysis is that the potential exists for the sample composition to change as a result of process upsets. For example, a sudden drop in temperature caused by clouds during the thermal reduction stage would shift the equilibrium in the direction of greater spinel in an $x \sim 1.0$ sample (Figure 7), leading to reduced H_2 production. How quickly the system recovers depends upon the kinetics of TR, but as the data in Figure 6 suggest, these are slow at 1673 K. Permanent deactivation of the system with respect to H_2 production might therefore occur, unless very high temperatures are used during the TR step (see below). In any case, measurements of the kinetics of spinel formation and subsequent reduction at high temperature would be invaluable in assessing the potential for this type of degradation.

Thermal Reduction. The features of the TR step in a thermochemical cycle are often the factors determining its success or failure as a practical system, because they determine the highest operating temperature of the system, which in turn affects the stability of other materials in the system, gas-flow or pumping requirements, and heat recuperation rates. Optimally, therefore, the solar-driven TR step in a thermochemical cycle using ferrites should possess the following properties to enable its practical application. First, it is desirable to maximize the oxygen partial pressure at temperatures generated by typical solar concentrators (1500−2000 K), so that dilution or pumping requirements are minimized. A $p(O_2)$ above that in air is optimal but not required. A second and related point is that TR should not require such high temperatures (even though these might be achievable in a solar concentrator) that other materials in the system are affected either chemically or mechanically. Collector losses also increase dramatically with increasing temperature. Third, the products of TR should be solids rather than liquids to maintain structural integrity of the system. Finally, fast decomposition kinetics are desirable to minimize cycle times. Thermodynamic modeling can provide useful guidance for all but the last of these.

To model the TR step for individual ferrites, we computed the equilibrium as a function of the temperature using an input mixture of 1 mol of the ferrite in an atmosphere of Ar. As in previous calculations, the pressure was held constant at 1 atm; the O_2 activity was allowed to vary. It is important to recognize that, although the chemical reactions can be fast at the high temperatures of this process, as indicated by the results discussed above, the experimental systems used to date to test ferrite thermochemical cycles do not operate at equilibrium (see for example refs 5−10). Gas flows within these reactors remove product oxygen gas, maintaining $p(O_2)$ at sub-equilibrium values, so that the reaction goes to completion. Consequently, we chose an input condition with a very high dilution (10^4 mol

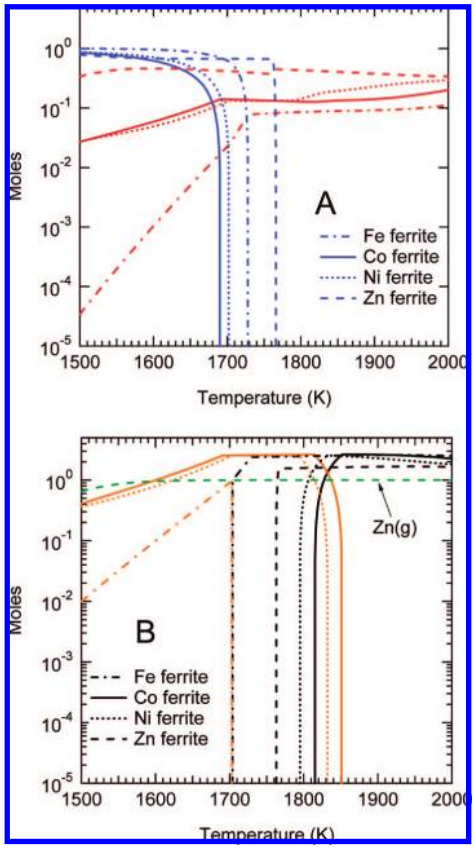

Figure 10. Equilibrium composition as a function of the temperature under thermal reduction conditions (input conditions: total pressure = 1 atm; Ar/MFe_2O_4 mole ratio = 10^4; O_2 activity variable). (A) Ferrite (blue) and O_2 (red). (B) MeO solid solution (all components, orange), Zn metal (green), and slag phase (black). The vertical line at 1705 K in B indicates the solid−liquid phase transition between the MeO solid solution and slag phases for Fe_3O_4.

of Ar/mol of MFe_2O_4) to simulate this situation. Note, however, that this choice is illustrative and not definitive. Increasing the Ar/MFe_2O_4 dilution shifts the spinel curve to lower temperatures (spinel is completely decomposed at 1780 and 1690 K at 10^3:1 and 10^4:1, respectively), while the temperature dependence of the slag and MeO phases is unchanged. This prediction is consistent with the experimental result reported by Han et al., who find that TR of $NiFe_2O_4$ in a flowing system can occur at temperatures of 1473 K (although the reduction may not be complete at this low temperature).[37] In the extreme case of very high dilution ($\geq 10^5$:1), considerable metal vaporization occurs (e.g., Fe and Ni) at high temperatures, which has been observed under some conditions in a solar reactor.[40]

The results of this thermodynamic modeling, shown in Figure 10, indicate that, at the temperatures of interest for solar TR (1500−2000 K), the four ferrites considered here display varying degrees of stability as a function of the temperature. That reduction occurs is evident from the formation of O_2 (Figure 10A). In general, the stabilities are $Fe_3O_4 > CoFe_2O_4 \sim NiFe_2O_4 > ZnFe_2O_4$, as measured by the relative amounts of O_2 formed at a given temperature. Clearly, the effect of metal substitution in Fe_3O_4 is to destabilize the spinel phase relative to a solution (either solid or liquid) of other metal oxides; i.e., the metal-substituted ferrites decompose at a lower temperature than Fe_3O_4. However, the condensed-phase products (Figure 10B) and relative temperatures at which a liquid slag phase form differ for these three material groupings and will likely be determining factors in the viability of each material for solar hydrogen generation.

Considering Fe_3O_4 first, it is evident why this material is not successful for solar hydrogen generation. Although it loses O_2 to form the MeO phase prior to forming liquid slag, the reduction is not complete until temperatures are above the melting point of the MeO phase. The formation of a liquid phase leads to sintering and gas-transport limitations that slow the reaction to unacceptable rates.[19,35] In contrast, the Co- and Ni-substituted ferrites are essentially fully decomposed at 1700 K and display a ~100 K region, in which the MeO phase is stable. In this region, the equilibrium concentration of O_2 (Figure 10A) is essentially constant, suggesting that there is little thermodynamic advantage to operating at the upper end of this temperature range. Higher temperatures may still be an advantage for increasing reaction rates, however.

Zinc ferrite is a special case among the four ferrites, displaying significantly different behavior with respect to temperature and the identity of the products formed. Unlike the other three ferrites, $ZnFe_2O_4$ does not decompose to a solid solution. Instead, it partially decomposes (<33 mol %) at $T <$ ~1760 K, forming gas-phase Zn and a Zn-depleted ferrite, rather than the MeO or zincite solid solution phases. Gas-phase metal atom concentrations for the other ferrite systems are predicted to be at least an order of magnitude lower than Zn(g) in this temperature range. At temperatures >1760 K, it melts to form a Zn−Fe−O slag. This unique behavior reflects the fact that Zn^{II}, with a fully filled d shell, does not behave chemically like other third-row transition metals. From a practical point of view, the high gas-phase Zn concentration is undesirable. In a flowing system, the ferrite will be permanently depleted of the zinc, leading to the formation of Fe_3O_4 upon thermal cycling. The temperature at which the slag phase forms, although considerably higher than for Fe_3O_4, is predicted to be much lower than either the Ni or Co ferrites. These predictions agree qualitatively with the experimental observations of Tamaura et al.,[10] who found ZnO deposited on the (cold) walls of their reactor. Their experimental results can be qualitatively reproduced by our equilibrium calculations. Quantitative agreement can be achieved as well, but approximately 100 times as much air must be used as they report.

Of the four ferrite systems considered here, therefore, the Ni- and Co-substituted ferrites are comparable with regard to the three thermodynamic-based criteria discussed at the beginning of this section, having properties that are superior to both $ZnFe_2O_4$ and Fe_3O_4. This conclusion is consistent with our preliminary investigation, which considered mixtures of MFe_2O_4 and zirconia used as a support.[36] In that case, $NiFe_2O_4$ appeared to be the best of the four systems, but predictions for $CoFe_2O_4$ were similar. The conditions of those simulations, which assumed a fixed reactor volume rather than a constant total pressure, as well as the inclusion of zirconia in the calculation, lead to equilibrium O_2 vapor pressures and slag-phase formation temperatures that are only slightly different than for the analogous $CoFe_2O_4$ mixture.

Water Oxidation. Efficient hydrogen production places several requirements on the system. The reaction must be spontaneous at the temperature of the water oxidation (WO) step for H_2 to be produced, and preferably, this should be the case at as low of a temperature as possible to maximize heat-transfer rates if thermal recuperation is used, as in the CR5 process. However, the kinetics of WO should also be fast, which in general requires WO to be performed at as high of a

(40) Siegel, N. Personal communication, 2008.

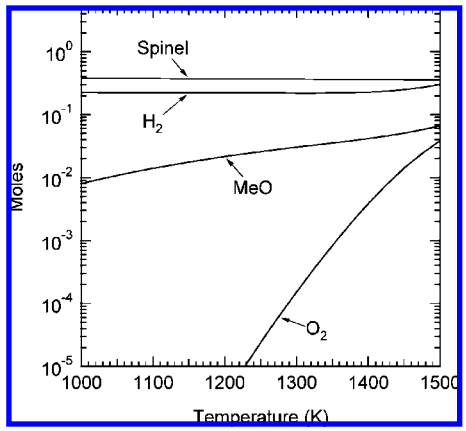

Figure 11. Composition of the solid and gas phases resulting from water oxidation in excess steam as a function of the temperature (P_{tot} = 1 atm) in excess steam (10^3/1 mol ratio). The input metal oxide mixture (CoFeO_TR1750 in the text) corresponds to the computed equilibrium at 1750 K of 1 mol of $CoFe_2O_4$ in 10^4 mol of Ar (see the text).

temperature as possible to minimize cycle times. These requirements are obviously conflicting; therefore, a compromise must be reached. Additionally, thermodynamic conditions for WO must be found, for which the spinel phase is the most stable one, so that essentially all of the reduced material formed by thermal reduction can be reconverted to ferrite. If such conditions cannot be found, the ferrite will be partially converted to another material with each cycle, resulting in the steady loss of hydrogen production efficiency if the reaction is not reversible. In this discussion, we focus on the $CoFe_2O_4$ system, which is similar to the $NiFe_2O_4$ previously analyzed and discussed in a preliminary report.[36]

As discussed above, TR of cobalt ferrite at temperatures below 1800 K yields the MeO solid solution of oxides (Co^{II}, Fe^{II}, and Fe^{III} in the MeO oxide solid solution), which is reoxidized by exposure to steam in the WO step. We modeled all four transition-metal ferrite systems and find similar behaviors when the mixture resulting from TR is exposed to excess steam. To model this process, two equilibrium calculations were performed. First, we computed and saved the mixture of phases resulting from TR of 1.0 mol of pure $CoFe_2O_4$ in dilute Ar (10^4 mol of Ar/1 mol of $CoFe_2O_4$; 1 atm total pressure; O_2 activity allowed to vary) at 1750 K and refer to this mixture as CoFeO_TR1750. At this TR temperature, the $CoFe_2O_4$ is entirely decomposed to MeO and no liquid slag phase forms at equilibrium. Second, we used CoFeO_TR1750 as the input to a second equilibrium calculation, in which excess steam (10^3 mol) was included in the 1000−1500 K temperature range (1 atm total pressure; O_2 activity allowed to vary). The resulting components in the mixture and the amounts of H_2 and O_2 produced as a result are plotted as a function of the WO temperature in Figure 11.

It is evident from Figure 11 that the spinel phase is the most stable at all temperatures, with only small amounts of the MeO solution forming, and that H_2 is produced as a result of the reoxidation of CoFeO_TR1750. These predictions are consistent with measurements reported by Aoki et al.,[8] whose results indicate that the WO step is fast and yields 90% of the theoretically possible amount of H_2. A slight decrease in the stability of the spinel with the temperature is predicted at the highest temperatures, as evidenced by increasing amounts of MeO solution components as the temperature increases. Even here, more than 85% of the condensed phase at 1500 K consists of spinel. Nevertheless, this result indicates it is preferable to operate the WO step at as low of a temperature as possible, heating the system only enough to achieve acceptable reaction rates.

Our previous analysis of the $NiFe_2O_4$ system indicates that some O_2 and H_2 exist at equilibrium as a result of the decomposition of gas-phase H_2O. However, the concentration is extremely small (<100 ppm at 1500 K). The results in Figure 11 show this as well. The amount of H_2 formed in the presence of CoFeO_TR1750 is significantly higher than the amount formed when only steam is included in the calculation, indicating that H_2 is produced by reoxidation of the MeO phase and not decomposition of H_2O. It is unlikely that this prediction would be realized in practice, because kinetic factors will likely limit the extent of H_2O decomposition. The prediction suggests, however, that there is an optimal temperature that maximizes H_2 production while minimizing or eliminating O_2. The presence of significant amounts of O_2 in the H_2 stream presents not only a potential safety hazard but also a separations problem, because the O_2 would have to be removed before the H_2 could be used as a fuel.

Conclusions

Thermodynamic modeling has long been used to guide the development of high-temperature processes. However, the complexity of the phase compositions that can occur in ferrite systems has been unappreciated, resulting in modeling approaches that are oversimplified. The results of this investigation demonstrate that thermodynamic modeling can be quite effective when applied to solar hydrogen generation, on the basis of comparisons with experimental data presented here and in the literature. Although thermodynamic data are not available for all systems of interest, they are sufficient to permit a detailed examination of several metal-substituted ferrites that are promising materials for this application. All aspects of the process related to the ferrites themselves (as opposed to external issues, such as heat transfer and the stability of nonredox materials that may be used in a solar heat engine) were considered in this investigation, including material synthesis, thermal reduction, and water oxidation.

A key conclusion of this investigation concerns the importance of including solution phases, which are shown to markedly affect the results of equilibrium calculations involving ferrites. To date, such phases have not been included in previously reported thermodynamic analyses,[9,19,20] with the exception of our preliminary report.[36] This leads to inaccurate predictions of, for example, the temperature at which liquid phases are expected to form. An additional misconception concerning ferrites related to the existence of solution phases is that these materials melt to form a liquid with the stoichiometry MFe_2O_4. While this is possible when the O_2 activity is fixed (i.e., the partial pressure of O_2 in the gas above the condensed phase is constant, as is the case for data reported in phase diagrams), under the conditions typically used for ferrite preparation and thermal reduction, they do not undergo a simple solid−liquid phase change (i.e., congruent melting). Instead, ferrites can lose oxygen to produce either a second solid solution (modeled here by the MeO and/or zincite phases) or, at higher temperatures, a liquid oxide slag phase.

This study also shows that the composition of prepared samples is quite sensitive to the conditions under which materials are prepared. The M/Fe ratio, temperature history, and gas composition all affect the composition of the final product. It is particularly important to note that if the reactor environment is not scrupulously free of O_2 during the cool-down phase

following calcination, other chemistries (e.g., the formation of Fe_2O_3) can result. However, if an input M/Fe ratio of 1.9−2.0 is used (0.95−1.0 mol of MO in the various figures shown here), the equilibrium composition is essentially fixed at MFe_2O_4, regardless of whether an inert gas or air is used during the cool-down phase. Thus, compositions, such as $Co_{0.67}Fe_{2.33}O_4$, that we employed in an earlier experimental investigation[18] are not desirable because the composition varies with temperature. In general, our results show that conditions must be carefully controlled throughout all stages of ferrite synthesis and during thermal cycling to produce hydrogen.

It is evident from this modeling that the thermal reduction step may be the determining factor in the success or failure of a chosen materials system, more so than the water oxidation step. Water oxidation is thermodynamically downhill for all ferrites considered here, such that essentially complete reconversion to the original ferrite occurs. The requirements for the reduction step, on the other hand, cannot be met by all materials. This step is also the one most likely to lead to deactivation of the ferrite because of potential reductions in transport rates caused by sintering. Alternatively, the temperature of the water oxidation step must be compatible with other materials used as supports and insulation. Of the ferrites considered here, the nickel and cobalt ferrites are similar and appear to have the best combination of properties for solar hydrogen generation. Neither Fe_3O_4 nor zinc-substituted ferrite is comparable. These predictions are fully consistent with reported experimental investigations of this class of redox materials.[7−11,13,41−44]

Acknowledgment. We are grateful to Ralph Tissot for conducting the XRD analysis used in this work and to Dr. T. M. Besmann and Prof. C. Wolverton for helpful technical discussions. This work is supported by the U.S. Department of Energy under contract DE-AC04-94-AL85000. Funding was provided by the Sandia National Laboratories Laboratory Research and Development Program.

EF8005004

(41) Aoki, H.; Kaneko, H.; Hasegawa, N.; Ishihara, H.; Suzuki, A.; Tamaura, Y. *Solid State Ionics* **2004**, *172*, 113.
(42) Hwang, G. J.; Park, C. S.; Lee, S. H.; Seo, I. T.; Kim, J. W. *J. Ind. Eng. Chem.* **2004**, *10*, 889.
(43) Inoue, M.; Hasegawa, N.; Uehara, R.; Gokon, N.; Kaneko, H.; Tamaura, Y. *Sol. Energy* **2004**, *76*, 309.
(44) Tamaura, Y.; Ueda, Y.; Matsunami, J.; Hasegawa, N.; Nezuka, M.; Sano, T.; Tsuji, M. *Sol. Energy* **1999**, *65*, 55.